Lévy random walks in finite systems

P. M. Drysdale* and P. A. Robinson†
School of Physics, University of Sydney, New South Wales 2006, Australia
(Received 18 May 1998)

Lévy walks on finite intervals with absorbing boundaries are studied using analytic and Monte Carlo techniques. The integral equations for Lévy walks in infinite 1D systems are generalized to treat the evolution of the probability distribution on finite and semi-infinite intervals. In particular the near-boundary behavior of the probability distribution and also its properties at asymptotically large times are studied. The probability distribution is found to be discontinuous near the boundary for Lévy walks in finite and semi-infinite systems. Previous results for infinite systems, and a previous scaling for semi-infinite systems, are reproduced. The use of linear operator theory to solve the integral equations governing the evolution of the Lévy walk implies that the probability distribution decays exponentially at large times. For a jump distribution that satisfies $\psi(x)\sim|x|^{-\alpha}$ for large $|x|$, the decay constant for the exponential decay is estimated and found to scale at large L as $L^{1-\alpha}$ for $2<\alpha<3$ and L^{-1} for $1<\alpha<2$, in contrast to L^{-2} for normal diffusion. For $2<\alpha<3$, the ratio of the decay constants of the first and second eigenfunctions is less than 4 for large L, so that the second eigenfunction is relatively more important in describing the system's large time behavior than the corresponding eigenfunction for normal diffusion. For $1<\alpha<2$ the ratio of the decay constants may be greater or less than 4. The shapes of the eigenfunctions for the Lévy processes are obtained numerically and the strong similarity between the first eigenfunction and its normal diffusion counterpart for $2\lesssim\alpha<3$ indicate that it would be difficult experimentally to distinguish such a Lévy process on a finite interval from a normal diffusive system by considering only the asymptotic shape of the probability distribution. For $\alpha\lesssim2$ we observe significant differences between the first and second eigenfunctions and their normal diffusion counterparts. For moderately large intervals, the first eigenfunction is flatter with large boundary discontinuities while the second eigenfunction can differ from its normal diffusion counterpart in both its symmetry properties and number of nodes. [S1063-651X(98)09210-1]

PACS number(s): 05.40.+j, 02.50.−r

I. INTRODUCTION

Diffusion processes are commonly modeled using random walks. A simple model for a diffusive random walk involves a walker that steps at regular time intervals with a specified probability distribution of step lengths (known as the jump distribution) that is independent of the current position of the walker. If the jump distribution possesses finite first and second moments, the evolution of the random walker's positional probability distribution can be described by the Fokker-Planck equation for diffusion with a constant diffusion coefficient [1].

Where a random walker's jump distribution does not possess a finite second moment, the central limit theorem cannot be used to describe the walker's motion in terms of a diffusion equation [2,3]. The motion of a random walker that steps at regular time intervals with a jump distribution not possessing a finite second moment is known as a Lévy flight [4] (alternative more restrictive definitions exist [5]). For a Lévy flight, the probability distribution of the walker's position can be represented by one of a set of distributions known as the Lévy stable distributions [2,3] after a large number of steps.

The theory of Lévy flights remained a mathematical curiosity with few physical applications for many years. The principal reason for this is the mean square displacement of the Lévy flight random walker diverges in a nonphysical manner at finite times. In order for Lévy flights to have physical applications, the mean squared displacement should not diverge within a finite time period. One method suggested for removing the nonphysicality of the Lévy flight is the truncated Lévy flight (TLF) model [6]. The TLF model replaces the jump distribution, which has a divergent second moment by a Lévy distribution truncated at large step sizes. The truncated Lévy distribution has a large but still finite second moment. The TLF model displays behavior similar to Lévy flights at short times but at asymptotically large times it is governed by the central limit theorem as are standard diffusive random walks. A more sophisticated method of dealing with the divergent mean square displacement in the Lévy flight model is the Lévy walk model [7], in which the time taken to complete a step depends on the step length, with longer steps taking more time. The Lévy walk couples the spatial and temporal aspects of the walker's motion so that the mean squared displacement cannot diverge within a finite time.

A consequence of the Lévy flight and Lévy walk models is that in general the evolution of the position of the random walker (in a probabilistic sense) must be described by integral equations rather than partial differential equations [8,9]. The primary difference between Lévy diffusion processes and normal diffusion is the scaling of the mean squared displacement with time. Normal diffusion processes have mean squared displacements $\langle r^2\rangle$ that increase only linearly with

*Electronic address: peter@physics.usyd.edu.au
†Electronic address: robinson@physics.usyd.edu.au

time. Lévy processes though can display superdiffusive properties so that $\langle r^2\rangle \sim t^\gamma$ with $\gamma > 1$ [10]. Random walks with subdiffusive behavior ($\gamma < 1$) have also been considered [11] but we do not consider such models in this paper. A Lévy walk differs from a Lévy flight in the sense that is not a Markovian process; i.e., the future motion of the random walker is not completely independent of its past history but possesses a memory since walkers continue in a fixed direction for a specified (sometimes large) distance between turning points. Lévy walks possess some similarities to Markovian processes since, at each turning point, the position of the random walker's next turning point is chosen independently of its past history. Lévy walks thus form a class of semi-Markovian processes [12].

The behavior of Lévy walks and flights is well understood in infinite one-dimensional (1D) systems [10]. Lévy flights in semi-infinite 1D systems have been considered by Zumofen and Klafter [5] in the special case where the jump distribution of the random walkers is itself a Lévy distribution. While the Lévy walk on a half axis is not as well understood, Zumofen and Klafter's numerical analysis also showed close analogies between the scaling behavior of Lévy flights and Lévy walks [5].

The main purpose of this paper is to determine the properties of Lévy walks on finite and semi-infinite intervals with absorbing boundaries. These problems are more representative of real physical situations than the case of a Lévy walk on an infinite interval, which has received the bulk of theoretical attention to date. The finite interval and the semi-infinite system are thus fundamental building-block cases in the theoretical and practical understanding of Lévy processes, as they are for standard diffusive random walks [1].

The structure of this paper is as follows. In Sec. II the basic theory of Lévy walks is reviewed and equations for the evolution for a Lévy walk on a finite interval are derived. In Sec. III we consider the behavior of the probability distribution near the boundaries for Lévy walks on finite and semi-infinite intervals. In Sec. IV the behavior of the turning point distribution of the Lévy walkers in the asymptotic limit of large times is considered. In Sec. V we consider the probability distribution of Lévy walkers, particularly in the asymptotic limit of large times.

II. THEORY OF LÉVY WALKS

In this section we derive the evolution equations for Lévy walks on a finite interval with absorbing boundaries. The discussion begins with the derivation of the equations of evolution for the so called *velocity model* for a Lévy walk.

In the velocity model the random walker is modeled as moving at constant velocity between turning points where it changes direction. At each turning point of its motion the random walker's next turning point is determined probabilistically by the jump distribution. Hence the probability that the random walker currently at a turning point will travel to its next turning point at a distance x in a time t is given by

$$\Psi(x,t) = \psi(x)\,\delta(|x| - vt), \tag{1}$$

where $\psi(x)$ is the jump distribution and $v \propto |x|^\beta$. In this paper we only consider the $\beta = 0$ case where the velocity of the walker is independent of the step size. Without loss of generality the units of time can then be rescaled to ensure $v = 1$. As noted in Sec. I, if $\psi(x)$ possesses a divergent second moment it gives rise to the properties of the system such as superdiffusion. For $\psi(x)$ to have a divergent second moment and to be monotonically decreasing for large $|x|$, we consider $\psi(x)$ such that $\psi(x) \sim |x|^{-\alpha}$ for large $|x|$, where $1 < \alpha < 3$. The index α is then used to classify Lévy processes, since their behavior in an infinite 1D system depends only on α after a large number of steps [2,3]. If we denote the turning point distribution by $Q(x,t)$, one has

$$Q(x,t) = \int_0^L \int_0^t Q(x',t')\Psi(x-x',t-t')\,dx'\,dt' + \delta(x-x_0)\,\delta(t), \tag{2}$$

on a finite interval $[0,L]$ with absorbing boundaries, where x_0 is the initial position of the walker. Equation (2) can be understood by noting that the integral term links the current turning point distribution to turning point distributions at previous times through the jump distribution. The delta function term corresponds to the initial position of the random walker [at $t = 0$ in Eq. (2)], when the integral term vanishes.

The probability distribution for the position of the random walker is given by

$$P(x,t) = \int_0^L \int_0^t Q(x',t')\Phi(x-x',t-t')\,dx'\,dt'. \tag{3}$$

Equation (3) expresses the fact that the particle is either at a turning point ($t = t'$) or has a probability $\Phi(x,t)$ of currently being at point x while traveling between turning points. The probability that the random walker is momentarily located at a given point while traveling between turning points is given by

$$\Phi(x,t) = \delta(|x| - t) \int_{|x|}^\infty \psi(x')\,dx'. \tag{4}$$

The integral equations of evolution (2)–(4) on a finite interval differ from the infinite medium equations through the existence of finite limits on the spatial integrals. The consequence of these finite limits is that, although Laplace transforms can be used to simplify the temporal aspect of the evolution equations (see below), the spatial component cannot be simplified using standard operator techniques (unlike the infinite case where Fourier techniques are conventionally employed [7,10]). After Laplace transforming (2) and (3), the evolution equations become

$$Q(x,s) = \int_0^L \Psi(x-x',s)Q(x',s)\,dx' + \delta(x-x_0), \tag{5}$$

$$P(x,s) = \int_0^L \Phi(x-x',s)Q(x',s)\,dx', \tag{6}$$

with

$$\Psi(x,s) = \psi(x)e^{-s|x|} \tag{7}$$

and

$$\Phi(x,s)=e^{-s|x|}\int_{|x|}^{\infty}\psi(x')dx'. \tag{8}$$

Although Eq. (5) has a kernel of a convolution type it is defined only on a finite interval and the kernel is not of a class for which exact solutions to the integral equation are known [13,14]. For any real s, Eq. (5) is a Fredholm equation of the second kind with a symmetric kernel whose solution can be expressed in terms of the eigenfunctions of the equation

$$\phi(x,s)=\lambda\int_0^L\Psi(x-x',s)\phi(x',s)dx', \tag{9}$$

where $1/\lambda$ is the eigenvalue [13]. The solution to Eq. (5), when s is real, may be expressed as

$$Q(x,s)=\sum_{i=1}^{\infty}\frac{\phi_i(x,s)}{\lambda_i(s)-1}\int_0^L\phi_i(x',s)\,\delta(x'-x_0)dx', \tag{10}$$

where $\phi_i(x,s)$ are the eigenfunctions of Eq. (9), and $1/\lambda_i$ are its eigenvalues [13].

Appendix A summarizes the principal properties of normal diffusive systems on finite intervals with absorbing boundaries, which are used for comparison purposes in this paper.

III. BEHAVIOR NEAR BOUNDARIES

In this section we consider the behavior of the turning point distribution near the boundaries of an interval. In Sec. III A we show that the turning point distribution has a finite discontinuity at the boundaries of the interval and consequently that the positional probability distribution of a random walker is discontinuous at the boundaries. In Sec. III B we consider the analogous result for a Lévy walk on a semi-infinite interval.

A. Behavior near a boundary of a finite interval

In order to deduce that the Laplace transformed turning point distribution $Q(x,s)$ is discontinuous at the boundary it is sufficient to show $Q(x,s)\geqslant C_1>0$ for all $0<x<L$ where C_1 is a constant. This ensures $\lim_{x\to 0}Q(x,s)\geqslant C_1>0$, whereas $Q(x,s)=0$ for $x<0$ and $x>L$.

Considering Eq. (5) and noting $\Psi(x,s)\geqslant\psi(L)e^{-sL}>0$, we find that

$$Q(x,s)\geqslant\psi(L)e^{-sL}\int_0^L Q(x',s)dx'. \tag{11}$$

Since $Q(x',s)$ is continuous, nowhere negative, and not everywhere zero for $s>0$, we have

$$\int_0^L Q(x',s)dx'>0. \tag{12}$$

If we define $C(s)$ by

$$C(s)=\psi(L)e^{-sL}\int_0^L Q(x',s)dx', \tag{13}$$

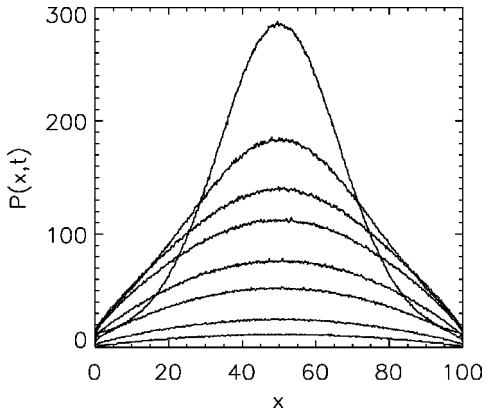

FIG. 1. Monte Carlo simulation of $P(x,t)$ at various times. The curves from top to bottom at the center correspond to $t=51$, 100, 150, 200, 300, 400, 600, and 800 respectively. The parameters are $\psi(x)=C(\alpha)(1+x^2)^{-\alpha/2}$, $L=100$, $\alpha=2.5$, and $x_0=50$. Boundary discontinuities can be seen at the edges.

we find

$$Q(x,s)\geqslant C(s)>0 \tag{14}$$

for all $0<x'<L$. Thus $Q(x,s)$ is discontinuous at the boundary for $s>0$.

The theorem of corresponding limits (p. 241 of Ref. [15]) states if $\lim_{x\to 0}f(x,s)=h(s)$ then $\lim_{x\to 0}f(x,t)=h(t)$ where $f(x,s),f(x,t)$ and $h(s),h(t)$ are Laplace transform pairs. Thus the discontinuities in $Q(x,s)$ at the boundaries imply corresponding discontinuities at the boundaries for $Q(x,t)$, for at least some times. From Eq. (6), each discontinuity in $Q(x,s)$ implies a discontinuity in $P(x,s)$. Hence the probability distribution $P(x,t)$ is also discontinuous at each boundary for at least some times. Such a discontinuity near a boundary can only occur after a time corresponding to the fastest time for a random walker to reach the boundary from its initial position. It is important to note the generality of the discontinuity result. If $\psi(L)\neq 0$, this is sufficient (though not necessary) for a discontinuity to arise. Since $\psi(L)\neq 0$ may be satisfied by jump distributions with finite second moments, a discontinuity can occur even if the system obeys ordinary diffusion. This would appear to contradict the standard solution to the usual diffusion equation given in Appendix A, which shows the probability distribution is always continuous near its boundaries. In fact there is no contradiction since, in the derivation of the ordinary diffusion equation, it is implicitly assumed not only that the second moment of the jump distribution is finite but that it is much smaller than the dimensions of the system so that $\psi(L)$ and the discontinuity are negligible. For Lévy flights the slower decay in the jump distribution increases the importance of the boundary discontinuity for finite L.

We now turn to our numerical results. To obtain the turning point and probability distributions numerically, Monte Carlo simulations with large ensembles of random walkers were performed. The Monte Carlo simulations were performed using systems where jump steps and hence time and space were discretized. Figure 1 shows results from a typical Monte Carlo simulation at moderately large L, shown for times after the first walkers reach the boundaries. The dis-

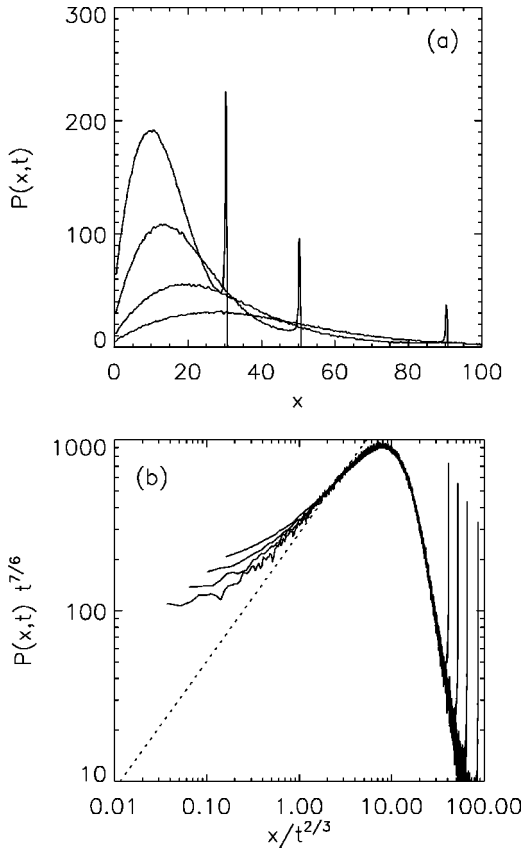

FIG. 2. Monte Carlo simulation of $P(x,t)$ in a semi-infinite 1D system. (a) $P(x,t)$ at various times. The curves from top to bottom at left correspond to $t=30$, 50, 90, 150, respectively, with parameters $\psi(x)=C(\alpha)(1+x^2)^{-\alpha/2}$, and $\alpha=2.5$. The boundary discontinuity can be seen at $x=0$. (b) $P(x,t)t^{1/2+1/(\alpha-1)}$ vs $x/t^{1/(\alpha-1)}$ at various t, showing collapse to Zumofen and Klafter's asymptotic scaling form. The curves from top to bottom at left correspond to $t=120$, 240, 480, 1080, respectively. The dashed line gives the theoretical near-boundary scaling. The parameters are $\psi(x)=C(\alpha)(1+x^2)^{-\alpha/2}$ and $\alpha=2.5$.

continuity at the boundary is clearly visible in the figure. After an initial increase the boundary discontinuity decays but as will be seen from the asymptotic analysis of $P(x,t)$ remains significant relative to $P(x,t)$ at all times.

B. Behavior near boundary for semi-infinite interval

For a Lévy walk on a semi-infinite interval, $Q(x,t)$ and $P(x,t)$ are discontinuous near the boundary for at least some times. This can be deduced from a variation of the proof given in Sec. III A. For Lévy flights it is similarly possible to show that a boundary discontinuity exists. Zumofen and Klafter's analytic analysis of Lévy flights considered the near-boundary behavior after asymptotically large times where the discontinuity vanishes. Nonetheless for finite times the boundary discontinuity can be significant. Zumofen and Klafter's numerical analysis of Lévy flights and walks (shown in Fig. 2 and Fig. 4 of Ref. [5]) at large but finite times generally agrees with the large time analytic predictions around the boundary but shows deviations from these predictions very near to the boundary. These deviations can be understood as arising from the boundary discontinuity. Zumofen and Klafter's numerical results show the relative significance of the boundary discontinuity decreases with time. Our numerical analysis confirms these conclusions, as shown in Fig. 2. Figure 2(a) shows a Monte Carlo simulation showing the boundary discontinuity decreasing in time. We note the peaks at large x seen in Fig. 2(a) correspond to random walkers at $|x|=t$, which are still moving to their first turning point. Analytically these peaks are delta functions, discretization leads to their finite height in the figure which is a measure of the relative area under them. Zumofen and Klafter argued that a data collapse to a universal asymptotic form should occur if $P(x,t)t^{1/2+1/(\alpha-1)}$ is plotted against $x/t^{1/(\alpha-1)}$. Figure 2(b) shows this collapse, thereby confirming the validity of Zumofen and Klafter's analytic and numerical analysis of the scaling behavior of $P(x,t)$. Very near to the boundary, $P(x,t)$ deviates from the predicted scaling due to the boundary discontinuity, as seen by the left hand end points of the curves in Fig. 2(b). The end point of each of the $P(x,t)$ curves corresponds to the same x, with the apparent horizontal movement due to the time-dependent scaling of the horizontal axis. From the figure we can infer at each value of the scaling parameter, $P(x,t)$ approaches the scaling form. Similarly for any value of x, the contribution of the boundary discontinuity relative to the peak of $P(x,t)$ decreases. Despite this the numerical results are inconclusive as to whether for any fixed value of x itself near the boundary, $P(x,t)$ approaches the scaling form, as the end points of the $P(x,t)$ curves do not appear to be approaching the scaling form.

IV. ASYMPTOTIC TEMPORAL BEHAVIOR

In this section we consider the asymptotic behavior of the turning point distribution at large times and contrast it with the behavior of normal diffusion processes governed by the diffusion equation. As the Laplace transformed turning point equation (5) is the simpler to work with, we need to derive the large-time behavior of $Q(x,t)$ from $Q(x,s)$. In Sec. IV A we deduce that to a good approximation the asymptotic time dependence of the $Q(x,t)$ involves exponential decay. In Sec. IV B an estimate for the decay constant of this decay is obtained using variational techniques and its scaling for large system sizes is considered. In Sec. IV C the eigenfunctions of the turning point equation are used to estimate the time required for the system to approach its asymptotic exponential behavior.

A. Asymptotic time dependence

In order to deduce the time-asymptotic behavior of the turning point distribution we require knowledge of the singularities of $Q(x,s)$. In Appendix B we deduce that the singularities of $Q(x,s)$ consist of a countably infinite set of simple poles along the real axis for negative s. Denoting the poles s_j so that they satisfy $|s_1|<|s_2|<\cdots$ we can then invert the Laplace transform for large times giving rise to

$$Q(x,t)\propto e^{-|s_1|t} \tag{15}$$

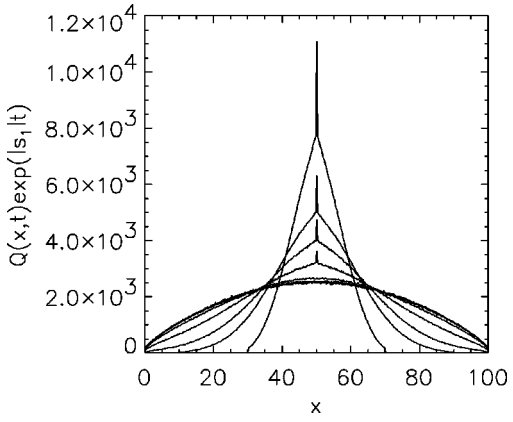

FIG. 3. The scaled turning point distribution $Q(x,t)e^{+|s_1|t}$ at various t. The curves from top to bottom at the center correspond to $t=20$, 40, 60, 100, 160, 260, 360, 460, respectively, for $\psi(x)=C(\alpha)(1+x^2)^{-\alpha/2}$, $L=100$, $\alpha=2.5$, and $x_0=50$.

for $t\to\infty$. This result is analogous to the dominance of the first eigenfunction in the time asymptotic behavior of a system undergoing normal diffusion [see Eq. (A2) in Appendix A].

In Fig. 3 we show numerical results for the scaled turning point distribution $Q(x,t)e^{+|s_1|t}$ at various times, calculated by Monte Carlo simulations. If Eq. (15) correctly predicts the asymptotic behavior of $Q(x,t)$, the graphs of $Q(x,t)e^{+|s_1|t}$ should coincide at large times. Figure 3 thus demonstrates the asymptotic behavior of the system is accurately described by the exponential decay given in Eq. (15). Note that in order to construct Fig. 3 a numerical value for $|s_1|$ was required. In this paper accurate positions for the singularities s_j are obtained through numerical inversion of Eq. (5). For $s\ll 1$ the numerical inversion is performed using the Nystrom method with Gauss-Legendre quadrature [16]. Where s does not satisfy $s\ll 1$, the product-Nystrom method [16] is used instead. The use of different methods of inversion for different regimes of s is required since the Nystrom method converges much slower than the product-Nystrom method if the kernel of the integral equation to be inverted has a sharp discontinuity in its derivatives. Where s is not small the kernel of Eq. (5) has a sharp discontinuity in its derivatives where $x=y$.

B. Estimated decay constant for exponential decay

This subsection estimates s_1, the decay constant for the principal eigenfunction, using a Rayleigh quotient variational technique. The Rayleigh quotient provides a lower bound on the largest eigenvalue based on a given estimated first eigenfunction (p. 63 of Ref. [13]). The Rayleigh quotient is equal to the first eigenvalue where the estimate for the first eigenfunction used is exactly the true first eigenfunction. In this subsection the normal diffusion first eigenfunction (A2) is used to approximate the first eigenfunction of the Lévy walk. The approximation made is likely to be most accurate as α approaches 3 from below, since for $\alpha>3$, the second moment of $\psi(x)$ becomes finite and for asymptotically large L such a system will undergo normal diffusion for large L.

The Rayleigh quotient is given by

$$R=\frac{\int_0^L\int_0^L \psi(|x-y|)e^{-s|x-y|}\sin(\pi x/L)\sin(\pi y/L)\,dx\,dy}{\int_0^L \sin^2(\pi x/L)\,dx}. \tag{16}$$

After changing variables and performing the integrations over $(x+y)$ in the numerator and over x in the denominator, we obtain

$$R=2\int_0^L \psi(u)e^{-su}\left\{\left[1-\frac{u}{L}\right]\cos\left(\frac{\pi u}{L}\right)+\frac{1}{\pi}\sin\left[\pi\left(1-\frac{u}{L}\right)\right]\right\}du. \tag{17}$$

At $s=s_1$, the Rayleigh quotient approximates $\lambda_1=1$ from below. By noting the Rayleigh quotient is a decreasing function of s, we can determine a lower bound approximation for s_1, by equating the Rayleigh quotient to unity and solving for s_1. Numerical simulations indicate for large L, $|s_1|\ll 1$, so assuming $|s|\ll 1$ one has $e^{-su}\simeq 1-su$, and we find

$$s_1\approx\frac{1-2\int_0^L B(u)\,du}{-2\int_0^L uB(u)\,du}, \tag{18}$$

$$B(u)=\psi(u)\left[\left(1-\frac{u}{L}\right)\cos\left(\pi\frac{u}{L}\right)+\frac{1}{\pi}\sin\left(\pi\frac{u}{L}\right)\right]. \tag{19}$$

In Appendix C we show that the estimate for s_1 can be expressed in terms of L as

$$s_1=\frac{\left(1/(\alpha-1)+\sum_{i=2}^{\infty} a_i/(i+1-\alpha)\right)A/L^{\alpha-1}-\sum_{i=2}^{\infty} a_i\Phi_i(0)/L^i}{\Phi_1(0)[A/(2-\alpha)]1/L^{\alpha-1}+\sum_{i=2}^{\infty} a_i\{[A/(i+2-\alpha)]1/L^{\alpha-2}-\Phi_{i+1}(0)/L^i\}}. \tag{20}$$

From Eq. (20), the estimated asymptotic scalings of s_1 at asymptotically large L are found to be

$$s_1 \propto \begin{cases} L^{-2}[1+o(1/L^{\min(\alpha-3,2)})], & \alpha>3 \\ L^{1-\alpha}[1+o(1/L^{\min(|3-\alpha|,|\alpha-2|)})], & 2<\alpha<3 \\ L^{-1}[1+o(1/L^{|2-\alpha|})], & 1<\alpha<2. \end{cases} \tag{21}$$

We note that a number of other approximations can be made for the true first eigenfunction of the system. However, provided the first eigenfunction can be expressed as a uniformly convergent power series and at large L approaches an asymptotic form expressible as a uniformly convergent power series in x, it can be shown that the scaling of s_1, in each regime will agree with the first term of the scaling given in Eq. (21), although the order of the correction terms may differ. [This result is subject to an additional assumption requiring the asymptotic form does not cause a term analogous to the bracketed term in the numerator of Eq. (20) to vanish.]

The scaling $s_1 \propto L^{-2}$ for $\alpha>3$ is expected since the jump distribution possesses a finite second moment in this regime and the random walk can be approximated by a normal diffusive random walk for large L (see Appendix A). The $s_1 \propto L^{1-\alpha}$ scaling for $2<\alpha<3$ demonstrates a fundamental difference between Lévy walk processes and normal diffusive processes, even at asymptotically large times. This $L^{1-\alpha}$ scaling is only accurate for very large L because the relative size of correction terms decreases no faster than $L^{-0.5}$. We consider the $\alpha<2$ scaling separately below.

In order to test the scaling for the decay constants, numerical inversion of the Laplace transformed turning point equation (5) was performed. Figure 4 compares the numerically obtained values of s_1 with the first order scaling given in Eq. (21) by dividing s_1 by the leading term on the right of Eq. (21) in each case and plotting the results against L. In each case, the results appear to approach a constant value as L increases, consistent with Eq. (21). As expected from Eq. (21) the correction terms are significant where L is only moderately large, so the results in Fig. 4 only asymptotically approach constant values. As Eq. (21) indicates, for $2<\alpha<3$, convergence to $s_1 \propto L^{1-\alpha}$ is fastest for $\alpha=2.5$ and slowest near $\alpha=2$ or $\alpha=3$. Figure 4(a) is consistent with this analysis as the convergence to asymptotically constant values is fastest for α nearer to $\alpha=2.5$ (where the results follow an almost horizontal line). Similarly Eq. (21) indicates for $1<\alpha<2$ that convergence to $s_1 \propto L^{-1}$ is fastest near $\alpha=1$, which is consistent with Fig. 4(b).

An estimate of s_1 at moderately large L values can be obtained analytically by computation of the coefficients in Eq. (20) or semianalytically by performing two numerical quadratures in Eq. (18) using a specified form of $\psi(x)$. Our numerical computations show that the fast semianalytic method for obtaining s_1 agrees with the more time-consuming method of numerical inversion of the turning point equation (5) to better than 15%, for moderately large L and $2<\alpha<3$. As expected, estimating s_1 using the normal diffusion first eigenfunction is most accurate for α near 3. For $2.5 \lesssim \alpha<3$, the relatively small error ($<5\%$) introduced by this approximation indicates the asymptotic shape of the turning point distribution is closely approximated by its normal diffusion counterpart. This error steadily increases as α decreases, indicating that the approximation using the normal diffusion eigenfuction breaks down for $\alpha \lesssim 2$. Nonetheless, the $s_1 \propto L^{-1}$ asymptotic scaling for $1<\alpha<2$ is still observed in Fig. 4(b), since this scaling is insensitive to the shape of the estimated eigenfunction, as noted earlier.

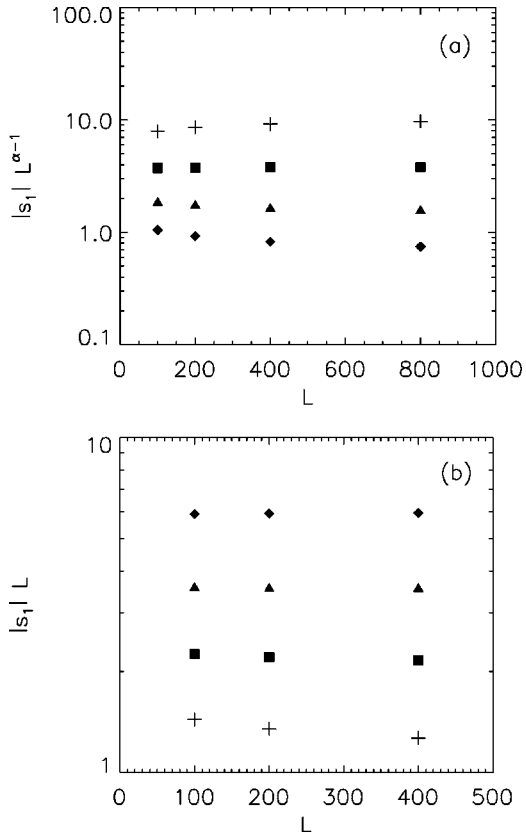

FIG. 4. The scaled decay constant vs L in various regimes. (a) $|s_1|L^{\alpha-1}$ vs L for $2<\alpha<3$ with $\psi(x)=C(\alpha)(1+x^2)^{-\alpha/2}$. The sets of points correspond to $\alpha=2.75$ (crosses), 2.5 (squares), 2.25 (triangles), and 2.05 (diamonds). (b) $|s_1|L$ vs L for $1<\alpha<2$ with $\psi(x)=C(\alpha)(1+x^2)^{-\alpha/2}$. The sets of points correspond to $\alpha=1.05$ (diamonds), 1.25 (triangles), 1.5 (squares), and 1.75 (crosses), respectively.

C. Time to approach asymptotic behavior

In this subsection the decay constant corresponding to the second eigenvalue of Eq. (9) is considered. The second decay constant s_2 provides a measure of the inverse of the time required for the system to approach its asymptotic behavior (i.e., the time after which its behavior is dominated by the first eigenfunction). The variational principle for obtaining the second eigenvalue analogously to the method used in Sec. IV C is known as the min-max principle (p. 63 of Ref. [13]). The min-max principle states the second eigenfunction maximizes the Rayleigh quotient over the set of functions orthogonal to the first eigenfunction. The Rayleigh quotient's maximum value over this set of functions is the second eigenvalue. Since the first eigenfunction is not known exactly, the use of the second normal diffusion eigenfunction as an approximation to obtain the second eigenvalue will provide only an estimate of the second eigenvalue rather than a rigorous bound. This is due to the fact that the second normal diffusive eigenfunction is not orthogonal to the first eigenfunction for the Lévy process so that the min-max principle does not strictly apply. Using the second normal diffusive eigenfunction as an approximation to obtain an estimate for s_2 in the same way that s_1 was estimated in Sec. IV C yields

$$s_2 \approx \frac{1-2\int_0^L D(u)du}{-2\int_0^L uD(u)du}, \tag{22}$$

$$D(u)=\psi(u)\left[\left(1-\frac{u}{L}\right)\cos\left(2\pi\frac{u}{L}\right)+\frac{1}{2\pi}\sin\left(2\pi\frac{u}{L}\right)\right], \tag{23}$$

and hence

$$s_2 \approx \frac{\left(1/\alpha-1+\sum_{i=2}^{\infty} b_i/i+1-\alpha\right)A/L^{\alpha-1}-\sum_{i=2}^{\infty} b_i\Phi_i(0)/L^i}{\Phi_1(0)-[A/(2-\alpha)]1/L^{\alpha-1}+\sum_{i=2}^{\infty} b_i([A/(i+2-\alpha)]1/L^{\alpha-2}-\Phi_{i+1}(0)/L^i)}, \tag{24}$$

where the b_i are now given by

$$\sum_{i=2}^{\infty} b_i u^i = 1-(1-u)\cos(2\pi u)-\frac{1}{2\pi}\sin(2\pi u). \tag{25}$$

The scaling of s_2 for large L is the same as for s_1 though the proportionality constants differ. For moderately large L and $2<\alpha<3$, our numerical studies indicate the decay constant s_2 can be estimated analytically or semianalytically in the same way as s_1, with similar accuracy to the s_1 estimates. It should be noted though, since the estimated second decay constant is not a bound but only an estimate, errors in the estimated value of s_2 include both underestimates and overestimates.

As noted in Appendix A, the ratio of s_2/s_1 for normal diffusion is 4. By comparing the ratio of the estimates of s_1 and s_2 given in Eqs. (20) and (24) for $2<\alpha<3$ we estimate

$$\lim_{L\to\infty}\frac{s_2}{s_1} \approx \frac{1/(\alpha-1)+\sum_{i=2}^{\infty} b_i/(i+1-\alpha)}{1/(\alpha-1)+\sum_{i=2}^{\infty} a_i/(i+1-\alpha)}. \tag{26}$$

Numerical evaluation of the series in Eq. (26) for $2<\alpha<3$ shows that the ratio is less than 4 and is a decreasing function of α. Convergence at moderately large L to this ratio is expected to be very slow for the same reasons that convergence to the asymptotic forms of s_1 and s_2 was slow due to the correction terms given in Eq. (21). For $\alpha>3$ the ratio of Eqs. (20) and (24) yields

$$\lim_{L\to\infty}\frac{s_2}{s_1}=\frac{b_2}{a_2}=4, \tag{27}$$

as is expected since the system behaves in a normal diffusive manner in this limit [cf. Eq. (A4)].

In order to study the ratio s_2/s_1 at moderately large L, the jump distribution $\psi(|x|)=C(\alpha)/(1+x^2)^{\alpha/2}$ was selected. [$C(\alpha)$ is the normalization constant and is given by $C(\alpha)=1/\beta[1/2,1/2(\alpha-1)]$, where β is the beta function, i.e., Euler's integral of the first kind]. Figure 5(a) shows the numerically calculated ratios of s_1 and s_2, relative to the semianalytic estimate obtained from numerical quadrature of Eqs. (18) and (22). As before, our estimates are most accurate for $2.5<\alpha<3$, whereas the accuracy decreases substantially as α decreases toward 2, as can be seen in the results for $\alpha=2.05$ in Fig. 5(a). Nonetheless the general trend shows that

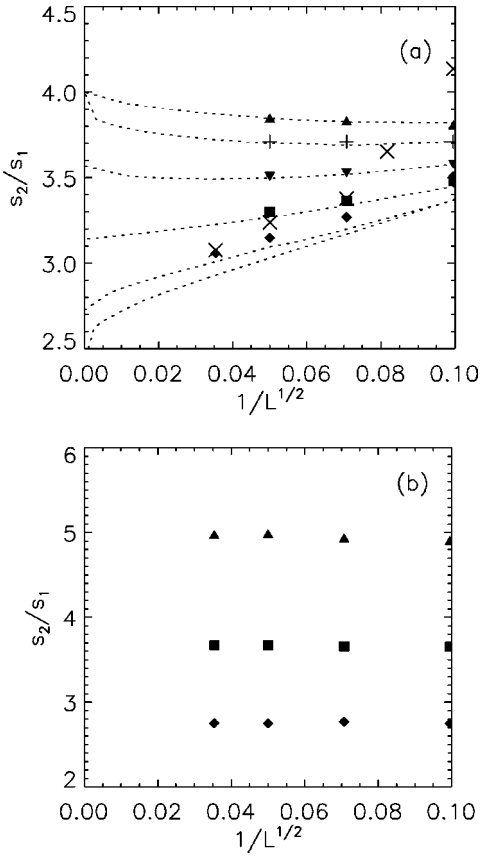

FIG. 5. Ratio of s_1 and s_2 for various L and α. The symbols denote the numerically calculated values. The dotted lines represent semianalytic estimates derived from numerical quadrature of the estimates (18) and (22) for s_1 and s_2. The dependent axis for (a) has been scaled to $L^{-1/2}$ in order to show the detail of the semianalytic estimates. The jump distribution for these simulations is $\psi(x)=C(\alpha)(1+x^2)^{-\alpha/2}$. (a) The points are $\alpha=3.25$ (triangles), 3.0 (plusses), 2.75 (inverted triangles), 2.5 (squares), 2.25 (diamonds), and 2.05 (crosses). (b) Same as (a) for $\alpha=1.75$ (triangles), 1.5 (squares), and 1.25 (diamonds), except that no semianalytic estimates are available for $1<\alpha<2$.

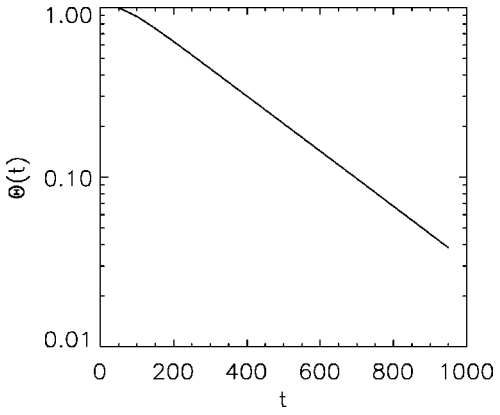

FIG. 6. Survival probability $\Theta(t)$ vs t for $\alpha=2.5$, $\psi(x)=C(\alpha)(1+x^2)^{-\alpha/2}$, $L=100$, and $x_0=50$.

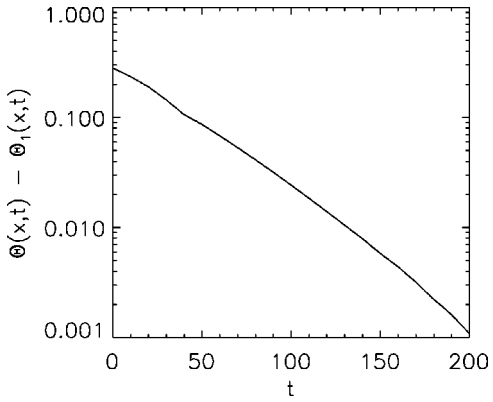

FIG. 7. Survival probability $\Theta(t)$ with first decay term $\Theta_1(t)$ removed. Parameters are $\alpha=2.5$, $\psi(x)=C(\alpha)(1+x^2)^{-\alpha/2}$, $L=100$, and $x_0=50$.

for moderately large interval sizes, the ratio s_2/s_1 decreases with decreasing α and approaches its asymptotic value only slowly. It is thus concluded at moderately large times the contribution of the second eigenfunction is more significant for $2<\alpha<3$ than for normal diffusion since its exponential decay is (relatively) slower. For $1<\alpha<2$ we do not possess an analytic estimate for s_1 and s_2 only the asymptotic scaling given in Eq. (21). Consequently we can make no analytic prediction relating to the ratio s_2/s_1 in the range $1<\alpha<2$. Figure 5(b) shows numerically calculated ratios of s_2 and s_1 at moderately large L. Unlike for $2<\alpha<3$, the ratio s_2/s_1 may be greater or less than 4 for $1<\alpha<2$ and hence the relative contribution of the second eigenfunction at moderately large times can be less significant than for normal diffusion (for $1<\alpha<2$ and near $\alpha=2$) but becomes more significant as the ratio s_2/s_1 decreases with decreasing α. Thus s_2/s_1 is decreasing in both the $2\lesssim\alpha<3$ and $1\lesssim\alpha\lesssim2$ regions, although since s_2/s_1 is greater at $\alpha=1.75$ than at $\alpha=2.05$, there is either a continuous or a discontinuous increase in s_2/s_1 for some part of $1.75\lesssim\alpha\lesssim2.05$.

V. PROBABILITY DISTRIBUTIONS

Having considered the asymptotic behavior of the turning point distribution in Sec. IV we now consider the asymptotic behavior of the probability distribution itself. Equations (6) and (8) connect the probability distribution with the turning point distribution. Since $\Phi(x,s)$ possesses no singularities for finite s, from Eq. (6) it can be seen that $P(x,s)$ has the same singularities for finite s as $Q(x,s)$. Hence $P(x,t)$ will have the same exponential decay behavior as that of $Q(x,t)$, with s_1 and s_2 playing similar roles. For example

$$P(x,t)\propto e^{-|s_1|t}, \tag{28}$$

as $t\to\infty$. If the probability that a random walker is still in the interval after a time t is termed the survival probability $\Theta(t)$, Eq. (28) predicts

$$\Theta(t)=\int_0^L P(x,t)dx,$$

$$\propto e^{-|s_1|t} \quad \text{for } t\to\infty. \tag{29}$$

Figure 6 shows the survival probability obtained from a typical Monte Carlo simulation, clearly showing exponential decay at large times. The decay constant for the exponential decay in Fig. 6 agrees with the independently calculated value for s_1, obtained through numerical solution of Eq. (5).

In order to determine the next term that contributes to the survival probability, we note when the second eigenfunction component of $Q(x,t)$ is closely approximated by its normal diffusion counterpart, the second eigenfunction is antisymmetric and does not contribute to the survival probability despite its contribution to $P(x,t)$. Thus, subtracting the contribution of the first decay term, $\Theta_1(t)$, from the survival probability isolates the next contribution to the survival probability; i.e., exponential decay at a rate given by the third decay constant, as is confirmed in Fig. 7. The decay constant observed in Fig. 7 is in agreement with s_3 calculated independently through numerical solution of Eq. (5). The deviation from exponential decay for $t\gtrsim120$ in Fig. 7 is due to inaccuracy in the estimation of the subtracted first decay term.

By considering an inner product of $P(x,t)$ with an estimate for the second eigenfunction the contribution of the second decay constant to the evolution of $P(x,t)$ can be demonstrated as shown in Fig. 8. The decay constant of the exponential decay observed in Fig. 8 agrees with s_2 calcu-

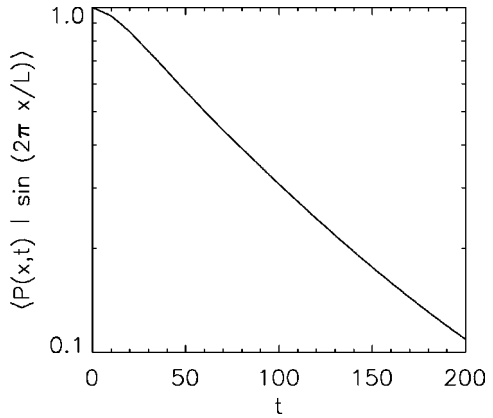

FIG. 8. Inner product of $P(x,t)$ with an estimate of the second eigenfunction, $\langle P(x,t)|\sin(2\pi x/L)\rangle$, demonstrating the contribution of the s_2 term to the evolution of $P(x,t)$. Parameters are $\alpha=2.5$, $\psi(x)=C(\alpha)(1+x^2)^{-\alpha/2}$, $L=100$, and $x_0=25$.

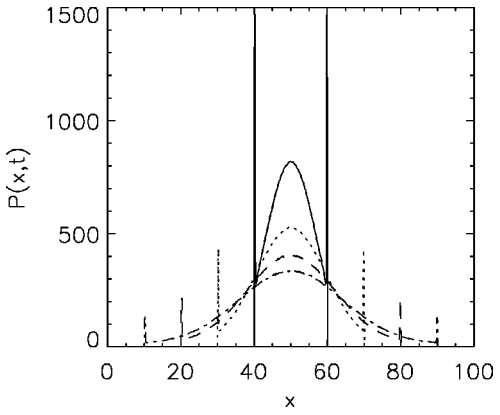

FIG. 9. Monte Carlo simulation of $P(x,t)$ at small t. Parameters are $\psi(x)=C(\alpha)(1+x^2)^{-\alpha/2}$, $L=100$, $\alpha=2.5$, and $x_0=50$, $t=10$ (solid), 20 (dotted), 30 (dashed), and 40 (dot-dashed).

lated independently through numerical solution of Eq. (5). The deviations from exponential decay visible in Fig. 8 are due to the inner product not completely excluding the contributions of the other decay terms to $P(x,t)$ because we use only an estimate for the second eigenfunction.

We consider the spatial variation of $P(x,t)$ next. For time periods less than the period for the fastest random walker to reach a boundary $P(x,t)$ evolves identically to the Lévy walk in the infinite 1D system, which was studied by Zumofen and Klafter [10]. This differs from a Lévy flight on a finite interval where $P(x,t)$ at no time evolves identically to the Lévy flight in the infinite 1D system. A typical Monte Carlo simulation for a Lévy walk on a finite interval at early times is shown in Fig. 9. It should be noted that the peaks on the leading edges of $P(x,t)$ are due to random walkers whose first step is very large and are still traveling to their first turning point. The area under the peaks diminishes in time and the peaks eventually leave the system. [Figure 1 shows the evolution of $P(x,t)$ after the peaks have left the system.]

For times $t \gg 1/s_2$, $P(x,t)$ approaches an asymptotic shape since $Q(x,t)$ is dominated by the first eigenfunction in this regime. The time asymptotic spatial form for $P(x,t)$ is related to the first eigenfunction of $Q(x,s)$ at $s=s_1$ through Eq. (5). Strictly speaking the spatial component of $P(x,t)$ decaying at a rate given by the first decay constant is not an eigenfunction since it is not the solution of an eigenvalue equation, but since it corresponds to the first eigenfunction in normal diffusion; we shall refer to it as the first ''pseudoeigenfunction.'' Figures 10(a) and 10(b) show the first pseudoeigenfunction component of $P(x,t)$ for $\alpha=2.5$ and $\alpha=1.75$ at various L. We note some general properties of the first pseudoeigenfunctions observed in numerical analysis and which are also evident in Figs. 10(a) and 10(b). For a given L, the size of the boundary discontinuity in the first pseudoeigenfunction increases with decreasing α. With increasing L the size of the boundary discontinuity decreases and at least for $\alpha>2$ it can be shown analytically that the boundary discontinuity vanishes as L becomes large. The asymptotic shape of the pseudoeigenfunction at large L is not precisely known, but our numerical analysis cannot rule out an approach to the normal diffusion first eigenfunction for large L for $\alpha>2$. There is a close similarity between the first

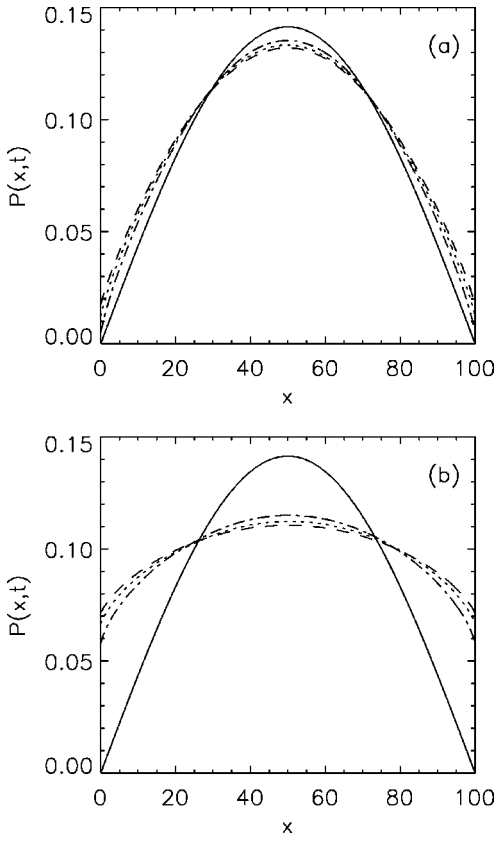

FIG. 10. Time-asymptotic shape for $P(x,t)$ at various L for $\psi(x)=C(\alpha)(1+x^2)^{-\alpha/2}$, $L=100$ (dashed), 200 (dotted), 1600 (dot-dashed). The normal diffusion first eigenfunction (A2) is included for comparison in each case (solid curve). (a) $\alpha=2.5$. (b) $\alpha=1.75$.

pseudoeigenfunction at large L for $2<\alpha<3$ and the normal diffusion eigenfunction, so it may be difficult in real physical systems to distinguish experimentally between Lévy walks and normal diffusion, by considering only the time asymptotic shape of $P(x,t)$. For $\alpha<2$ [see Fig. 10(b)] it appears considerably less likely that the pseudoeigenfunction approaches the diffusive one.

We now note some general properties of the second pseudoeigenfunction. For $2<\alpha<3$ the second eigenfunction for normal diffusion is a close approximation to the second ''pseudoeigenfunction,'' but as α approaches 2 at moderately large L, this approximation deteriorates and the second pseudoeigenfunction may even differ in the number of nodes it possesses compared to the second eigenfunction for normal diffusion [13]. This behavior continues for $1<\alpha<2$ even at very large L. Although this might at first appear a surprising result it is consistent with the fact that for $1<\alpha<2$ the integral operator in Eq. (9) is not ''oscillatory'' at s_2 in the sense of Ref. [13], even for large L. Only for an ''oscillatory'' operator is it guaranteed that the nth eigenfunction will have $(n-1)$ nodes. Figure 11(a) shows an example of the second pseudoeigenfunction for $\alpha=2.5$, where it is similar in form to the second eigenfunction for normal diffusion. Figure 11(b) shows an example of a second pseudoeigenfunction, which has two nodes rather than one. Note that this pseudoeigenfunction would contribute to the survival probability $\Theta(t)$ because it is symmetric, rather than

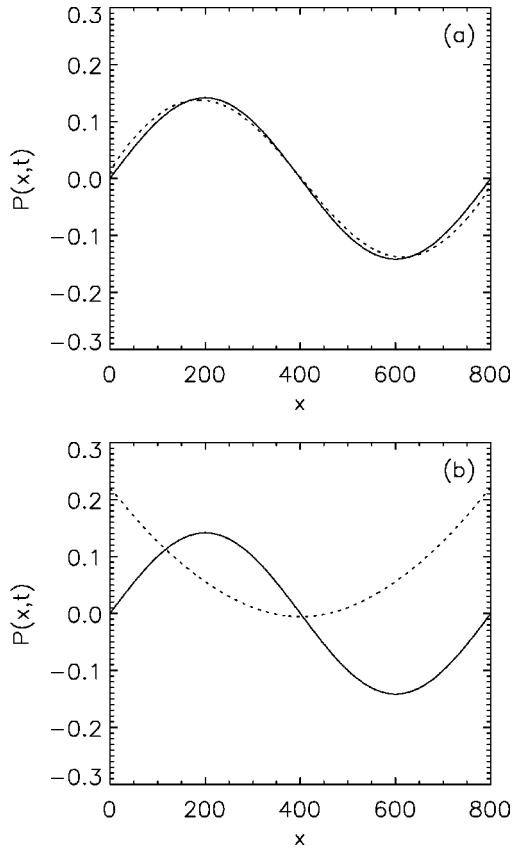

FIG. 11. The second pseudoeigenfunction of $P(x,t)$ for $\psi(x) = C(\alpha)(1+x^2)^{-\alpha/2}$, $L=800$ (dashed). The normal diffusion second eigenfunction (A2) is included for comparison in each case (solid curve) (a) $\alpha=2.5$. (b) $\alpha=1.75$.

antisymmetric. This pseudoeigenfunction cannot approach the diffusive second eigenfunction at large L unless the pseudoeigenfunction changes its topology from symmetric to antisymmetric at some large L.

VI. SUMMARY AND CONCLUSIONS

We have studied the behavior of Lévy walks on finite intervals with absorbing boundary conditions, considering in particular the near-boundary and asymptotically large time behavior using analytic, Monte Carlo, and numerical inversion techniques. Lévy walks of this type are fundamental building blocks in the understanding of Lévy processes in physical situations, where boundaries are present.

The main results of this paper are as follows:

(i) Initially the Lévy walk on the finite interval evolves in the same way as for the infinite system. For times shorter than the period for the fastest random walkers to reach the boundaries, $P(x,t)$ possess spikes at its edges corresponding to the random walkers still traveling to their first turning point. Eventually these spikes leave the system. After the spikes have left the system the probability distribution for Lévy walks is discontinuous at the boundaries for both finite and semi-infinite systems. For the finite system, this can significantly affect the system description at moderately large interval sizes, where the boundary discontinuities can be relatively large. For a Lévy walk on a finite interval the size of the discontinuity relative to $P(x,t)$ need not become insignificant even at asymptotically large times.

(ii) At asymptotically large times the Lévy walk probability distribution decays exponentially in magnitude on the interval, as does the total survival probability that random walkers remain on the interval. This is a consequence of the dominance of the first eigenfunction of the turning point distribution at large times.

(iii) For a jump distribution that satisfies $\psi(x)\sim|x|^{-\alpha}$ for large $|x|$, the scaling of the exponential decay constant was estimated as $s_1\propto L^{1-\alpha}$ for $2<\alpha<3$ and $s_1\propto L^{-1}$ for $1<\alpha<2$. These scalings show a fundamental difference between Lévy walks and the asymptotic time behavior of normal diffusion processes, which have $s_1\propto L^{-2}$.

(iv) As in normal diffusion, the decay constant corresponding to the second eigenfunction provides an estimate of the time before the system reaches its asymptotic regime. Analysis of the ratio of the first and second decay constants indicates that for $2<\alpha<3$ this ratio is smaller for Lévy walks than for normal diffusion, so that at moderately large times the contribution of the second eigenfunction is more significant since its exponential decay is relatively slower. For $1<\alpha<2$ the ratio can be larger or smaller than for normal diffusion, but decreases with decreasing α.

(v) The high degree of similarity between the first eigenfunctions of the Lévy walk and normal diffusion for large L and $2\leqslant\alpha<3$ suggest it would be difficult to experimentally differentiate such a Lévy walk on a finite interval from normal diffusion by considering only the differences in the asymptotic shape of the probability distribution. The most characteristic difference between the Lévy walk (for $2<\alpha<3$ and large L) is the difference in the scaling of the decay constant with system size. For $1<\alpha<2$ the first eigenfunction at moderately large L differs significantly from its normal diffusion counterpart, having large boundary discontinuities relative to its overall size and so it is consequently flatter than the normal diffusion first eigenfunction. The second eigenfunction, for large L and $1<\alpha<2$ can differ from the normal diffusive case so significantly that it can have different symmetry properties and a different number of nodes than the second eigenfunction of the normal diffusive system.

ACKNOWLEDGMENT

This work was supported by the Australian Research Council and the Australian Postgraduate Award Scheme.

APPENDIX A: REVIEW OF KEY RESULTS FOR NORMAL DIFFUSION ON A FINITE INTERVAL

In this Appendix we review the theory of normal diffusion on a finite interval with absorbing boundaries. The probability distribution for normal diffusion on a finite interval is given by the solution of

$$\frac{\partial P(x,t)}{\partial t} = D\frac{\partial^2 P(x,t)}{\partial x^2}, \tag{A1}$$

where D is the diffusion coefficient. For a finite interval $[0,L]$ with absorbing boundaries, Eq. (A1) is solved subject to the conditions $P(x,0)=\delta(x-x_0)$ and $P(x,t)=0$ for x

$\leqslant 0$ or $x \geqslant L$. The derivation of Eq. (A1) requires not only that the second moment of the jump distribution be finite but also tends to zero relative to L^2 [1,17]. The solution of Eq. (A1) can be expressed in terms of its eigenfunctions as [1]

$$P(x,t) = \sum_{n=1}^{\infty} A_n \sin(n\pi x/L) e^{-s_n t}, \tag{A2}$$

where $s_n = Dn^2\pi^2/L^2$. We note a number of properties of this probability distribution: (i) From Eq. (A2) it can be seen that $P(x,t)$ is always continuous at the boundaries. (ii) For asymptotically large times we find

$$P(x,t) \propto e^{-s_1 t}. \tag{A3}$$

(iii) The ratio of the first two decay constants is given by

$$\frac{s_2}{s_1} = 4. \tag{A4}$$

Since Lévy processes are more easily discussed primarily in Laplace transformed form, we note for that the Laplace transform of $P(x,t)$ is

$$P(x,s) = \sum_{n=1}^{\infty} A_n \sin(n\pi x/L) \frac{1}{s+s_n}. \tag{A5}$$

APPENDIX B: SINGULARITIES OF THE TURNING POINT DISTRIBUTION

In this Appendix we deduce the positions and properties of the singularities of $Q(x,s)$. This enables us to determine the asymptotic properties of $Q(x,t)$ at large times.

The Fredholm alternative theorem [13] guarantees a Fredholm equation of the second kind such as Eq. (5) possesses a unique solution except where its homogeneous eigenvalue equation has a nontrivial solution. The $\lambda = 1$ form of Eq. (9) is the corresponding homogeneous eigenvalue equation for Eq. (5). Hence $Q(x,s)$ will possess singularities for those values of s for which Eq. (9) possesses an eigenvalue equal to unity. For each real value of s the kernel of Eq. (9) is symmetric and bounded. Hence for real s the integral operator for the equation is self-adjoint and Eq. (9) has at most a countable set of eigenvalues, which if they approach a point as a limit, can only approach zero as a limit point. Here we assume that Eq. (9) has a countably infinite set of eigenvalues.

For each real value of s the kernel of Eq. (9) is positive everywhere and the integral operator is thus termed positive itself. For such a linear operator the eigenvalues satisfy

$$\frac{1}{\lambda_i} \leqslant \frac{1}{\lambda_1} \leqslant \max_{x \epsilon [0,L]} \int_0^L K(x,y)\,dy, \tag{B1}$$

where $1/\lambda_i$ are the eigenvalues and $1/\lambda_1$ is the first eigenvalue [13]. Hence we have

$$\frac{1}{\lambda_1} \leqslant \int_{-L/2}^{L/2} \psi(|y|) e^{-s|y|}\,dy. \tag{B2}$$

Since $\psi(y)$ is normalized on the interval $(-\infty,\infty)$, Eq. (B2) demonstrates that singular points of $Q(x,s)$ can exist only for negative s where the largest eigenvalue can be greater than unity. For increasingly negative s the bound on the largest eigenvalue increases. We assume then as s becomes increasingly negative, each eigenvalue increases and gives rise to a singularity when it is equal to unity and hence a countably infinite series of singularities corresponding to eigenvalues equal to unity exists for negative s. This assumption is plausible since, as we note below, each of the singularities of $Q(x,s)$ are isolated and there are at most a countably infinite set of singularities. Further for $\alpha > 3$, $P(x,s)$ and $Q(x,s)$ have a countably infinite set of singularities. Since a continuous change in α will yield a continuous change to the singularities on physical grounds, $P(x,s)$ and $Q(x,s)$ will thus also have a countably infinite set of singularities for a finite range of α with $\alpha < 3$.

At this point it remains possible that $Q(x,s)$ possesses singularities not on the real axis and we eliminate this possibility in the next few paragraphs. Since $Q(x,s)$ is defined off the real axis by analytic continuation, $Q(x,s)$ satisfies Eq. (5) for complex s. Thus the Fredholm alternative theorem guarantees that complex singularities in $Q(x,s)$ can only exist where Eq. (9) has an eigenvalue equal to unity for a complex s. Thus we need to obtain those s for which Eq. (9) has an eigenvalue equal to unity.

It can be shown the set of values of s (in general both complex and real) for which Eq. (9) has an eigenvalue equal to unity is closed and discrete so that each singularity of $Q(x,s)$ is isolated and there are only a countable number of these. The proof of this relies on spectral theory of analytic functions into Banach algebras, the details of which can be found in Chap. 3 of Ref. [18], especially the discussion relating to Theorem 3.4.26 in this reference. Since $Q(x,s)$ has a countable infinite set of singularities on the real axis there is at most a finite set of isolated complex singularities. It is assumed that the isolated singularities are not essential singularities.

Since $Q(x,s)$ is real for real s and defined by analytic continuation to the remainder of the complex plane, the complex singularities of $Q(x,s)$ are symmetric about the real axis. If $Q(x,s)$ possessed a complex singularity such that $\mathrm{Re}(s_j) > 0$, this singularity would contribute a residue with a component that grows exponentially with time. The nonphysicality of this behavior leads to the conclusion that $Q(x,s)$ cannot have any complex singularities with $\mathrm{Re}(s_j) > 0$. Considering complex singularities s_j such that $\mathrm{Re}(s_j) \leqslant 0$, and $|\mathrm{Im}(s_j)| > 0$, we note that each pair of such complex singularities s_j and s_j^* would contribute an oscillatory term in the Laplace inversion of the form

$$\mathrm{Res}(s_j + s_j^*) \propto G_j(x) t^{m_j} e^{-|\mathrm{Re}(s_j)|t} \cos[\mathrm{Im}(s_j)t], \tag{B3}$$

where $G_j(x)$ is the spatial term associated with the singularity. Since each of the possible complex singularities is isolated, we can sum the singularities $s_j = a_j + b_j i$ to give

$$Q(x,t) \propto \sum_j G_j(x) t^{m_j} e^{-|a_j|t} \cos(b_j t) + F(x,t), \tag{B4}$$

where $F(x,t)$ is the contribution from the singularities on the real axis and thus is not oscillatory. Since $Q(x,t)$ is a turning point distribution for a diffusionlike process, on physical grounds $\int Q(x,t)dx$ must be a monotonic decreasing function of time. But this implies the b_i are all zero, otherwise oscillatory behavior at the beat frequencies will arise among the terms in $\int Q(x,t)dx$. It is thus concluded that all singularities of $Q(x,s)$ must lie on the real axis.

Now that the positions of the singularities have been determined, it will be shown that each of the singularities is a simple pole. Denoting by s_j a singularity of $Q(x,s)$ lying on the negative real axis, we consider the eigenvalues, $1/\lambda$, and eigenfunctions in a neighborhood of s_j. If we restrict our attention to a neighborhood that lies on the real axis of s, we can expand the eigenvalue and eigenfunction in perturbation series in the usual way since the kernel is symmetric in this neighborhood. This yields

$$\sum_{i=0}^{\infty} \varepsilon^i \phi_i(x) = \sum_{i=0}^{\infty} \varepsilon^i \lambda_i \int_0^L \psi(|x-y|) e^{-(s_j+\varepsilon)|x-y|} \times \sum_{j=0}^{\infty} \varepsilon^j \phi_j(y). \tag{B5}$$

Equating linear terms in ε yields

$$\phi_1(x) = -\lambda_0 \int_0^L \psi(|x-y|) e^{-s_j|x-y|} |x-y| \phi_0(y) dy + \lambda_1 \phi_0(x) + \lambda_0 \int_0^L \psi(|x-y|) e^{-s_j|x-y|} \phi_1(y) dy. \tag{B6}$$

We now consider whether λ_1 vanishes in the neighborhood of any of the singularities. For λ_1 to vanish the equation

$$\phi_1(x) = \lambda_0 \int_0^L \psi(|x-y|) e^{-s_j|x-y|} \phi_1(y) dy - \lambda_0 \int_0^L \psi(|x-y|) e^{-s_j|x-y|} |x-y| \phi_0(y) dy \tag{B7}$$

must have a solution for $\phi_1(x)$. The Fredholm theorems [13] state if Eq. (B7) has a solution it is necessary that

$$\int_0^L \left(\lambda_0 \int_0^L \psi(|x-y|) e^{-s_j|x-y|} |x-y| \phi_0(y) dy \right) \times \phi_0(x) dx = 0. \tag{B8}$$

We will prove that there is no nontrivial function $\phi(x)$ that is symmetric or antisymmetric on $[0,L]$ and satisfies

$$\int_0^L \int_0^L \psi(|x-y|) e^{-s_j|x-y|} |x-y| \phi(x) \phi(y) dx dy = 0. \tag{B9}$$

This is sufficient to show that there is no solution for $\phi_1(x)$ and that λ_1 does not vanish since $\phi_0(x)$ is an eigenfunction and so is either symmetric or antisymmetric on $[0,L]$. By noting that $\psi(|x-y|)e^{-s_j|x-y|}$ has positive upper and lower bounds on $[0,L]$ and applying integral inequalities, the criterion in Eq. (B9) can be reformulated so that it is sufficient to show there is no nontrivial $\phi(x)$ that is symmetric or antisymmetric on $[0,L]$ and satisfies

$$\int_0^L \left(\int_0^L |x-y| \phi(x) dx \right) \phi(y) dy = 0. \tag{B10}$$

By noting that the Picard equation for an interval, given by

$$\int_0^L |x-y| \phi(y) dy = f(x), \tag{B11}$$

has a solution that must satisfy $\phi(x) = f''(x)/2$ [14], Eq. (B10) can be reformulated as

$$\int_0^L f''(x) f(x) dx = 0. \tag{B12}$$

Integrating by parts then yields

$$f'(L) f(L) - f'(0) f(0) - \int_0^L [f'(x)]^2 dx = 0. \tag{B13}$$

Since $\phi(x) = f''(x)$ is symmetric or antisymmetric on the interval $[0,L]$, and $f'(x)$ also must have the same symmetry or antisymmetry and thus Eq. (B13) requires $f'(x)$ to vanish on $[0,L]$ and hence $\phi(x)$ to vanish also. Thus there is no nontrivial $\phi(x)$ satisfying Eq. (B9) with appropriate symmetry. It has thus been proved that λ_1 does not vanish in the neighborhood of s_i.

At every singularity we conclude that the eigenvalue can be expressed as

$$\lambda(s) = 1 + (s-s_j)\lambda_1 + o[(s-s_j)^2] \tag{B14}$$

for real s where $\lambda_1 \neq 0$. For real s, Eq. (10) becomes

$$Q(x,s) \approx \frac{\phi_j(x_0,s)\phi_j(x,s)}{\lambda_1\{s-s_j+o[(s-s_j)^2]\}}. \tag{B15}$$

By analytic continuation, Eq. (B15) extends to complex s in the vicinity of s_j and each singularity is thus a simple pole.

The conclusion of this Appendix is that the turning point distribution $Q(x,s)$ has a countably infinite set of singularities for negative s which are all simple poles.

APPENDIX C: SCALING OF DECAY CONSTANT WITH SYSTEM SIZE

In this Appendix the scaling for the estimated decay constant with system size is obtained by considering Eq. (18).

If we denote the numerator of Eq. (18) by N we find

$$N = 1 - 2\int_0^L \psi(x) dx - 2\int_0^L \psi(x) G(x) dx, \tag{C1}$$

$$G(x) = \left(1 - \frac{x}{L}\right) \cos\left(\frac{\pi x}{L}\right) + \frac{1}{\pi} \sin\left(\pi \frac{x}{L}\right) - 1. \tag{C2}$$

Assuming L is sufficiently large that $\psi(L) \propto L^{-\alpha}$, we define A through the relation $\psi(x) = Ax^{-\alpha}$ for large x. Hence

$$N = 1 - \left[1 - \frac{2A}{\alpha - 1} \frac{1}{L^{\alpha-1}} \right] + 2 \int_0^L \psi(x) \sum_{i=2}^{\infty} \frac{a_i}{L^i} x^i dx, \tag{C3}$$

where the a_i are the Taylor coefficients, defined by

$$\sum_{i=2}^{\infty} a_i u^i = 1 - (1-u)\cos(\pi u) - \frac{1}{\pi}\sin(\pi u). \tag{C4}$$

Defining $\Phi_i(x)$ through the relation $\Phi_i(x) = \int \psi(x) x^i dx$, we then have

$$N = \frac{2A}{\alpha - 1} \frac{1}{L^{\alpha-1}} + 2 \sum_{i=2}^{\infty} \frac{a_i}{L^i} [\Phi_i(L) - \Phi_i(0)]. \tag{C5}$$

Assuming L is sufficiently large that $\psi(L) \propto L^{-\alpha}$, asymptotically we find $\Phi_i(L) = C_i + AL^{i+1-\alpha}/(i+1-\alpha)$. Without loss of generality we can define $C_i = 0$, which corresponds to assigning an arbitrary value to the integration constant for $\Phi(x)$ in the definition $\Phi_i(x) = \int \psi(x) x^i dx$. This yields

$$N = \left(\frac{1}{\alpha - 1} + \sum_{i=2}^{\infty} \frac{a_i}{i + 1 - \alpha} \right) \frac{2A}{L^{\alpha-1}} - \sum_{i=2}^{\infty} a_i \frac{2\Phi_i(0)}{L^i}, \tag{C6}$$

where the $\Phi_i(0)$ are constants that depend on the small x behavior of $\psi(x)$.

We now consider the denominator of Eq. (18), which we denote by D. We find

$$D = -2 \int_0^L \psi(x) x dx + 2 \int_0^L \psi(x) x \sum_{i=2}^{\infty} a_i \frac{x^i}{L^i} dx. \tag{C7}$$

Using the same notation as in Eq. (C6) then yields

$$D = -\frac{2A}{2 - \alpha} \frac{1}{L^{\alpha-1}} + 2\Phi_1(0) + \sum_{i=2}^{\infty} a_i \left[\frac{2A}{i + 2 - \alpha} \frac{1}{L^{\alpha-2}} - \frac{2\Phi_{i+1}(0)}{L^i} \right]. \tag{C8}$$

Using Eqs. (C6) and (C8) in Eq. (18) we find that the decay constant for the asymptotic exponential is given by Eq. (20).

[1] C. W. Gardiner, *Handbook of Stochastic Methods for Physics, Chemistry and the Natural Sciences* (Springer-Verlag, Berlin, 1983).

[2] P. Lévy, *Théorie de l'Addition des Variables Aléatoires* (Gauthier-Villars, Paris, 1937).

[3] W. Feller, *An Introduction in Probability Theory and Applications*, 2nd ed. (Wiley, New York, 1971), Vol. 2.

[4] M. Shlesinger, G. M. Zaslavsky, and J. Klafter, Nature (London) **363**, 31 (1993).

[5] G. Zumofen and J. Klafter, Phys. Rev. E **51**, 2805 (1995).

[6] R. N. Mantegna and H. E. Stanley, Phys. Rev. Lett. **73**, 2946 (1995).

[7] M. F. Shlesinger, B. J. West, and J. Klafter, Phys. Rev. Lett. **58**, 1100 (1987).

[8] V. Seshadri and B. J. West, Proc. Natl. Acad. Sci. USA **79**, 4501 (1982).

[9] V. M. Zolotarev, Dokl. Akad. Nauk SSSR **98**, 735 (1954).

[10] G. Zumofen and J. Klafter, Phys. Rev. E **47**, 851 (1993).

[11] M. F. Shlesinger, J. Klafter, and Y. M. Wong, J. Stat. Phys. **27**, 499 (1982).

[12] B. D. Hughes, *Random Walks and Random Environments* (Oxford Science, Oxford, 1995), Vol. 1.

[13] P. P. Zabreyko, A. I. Koshelev, M. A. Krasnosel'skii, S. G. Mikhlin, L. S. Rakovshchik, and V. Ya. Stet'senko, *Integral equations – A Reference Text* (trans. Noordhoff International, Leydon, 1975).

[14] H. M. Srivastava, and R. G. Buschman, *Theory and Applications of Convolution Integral Equations* (Kluwer Academic, Dordrecht, 1992).

[15] G. Korn and T. Korn, *Mathematical Handbook for Scientists and Engineers*, 2nd ed. (McGraw-Hill, New York, 1968), p.241.

[16] W. H. Press, S. A. Teukolsky, W. T. Vetterling and B. P. Flannery *Numerical Recipes in Fortran*, 2nd ed. (Cambridge, Cambridge, 1992).

[17] F. Spitzer, *Principles of Random Walk*, 2nd ed. (Springer-Verlag, New York, 1976), p. 244.

[18] B. Aupetit, *A Primer on Spectral Theory* (Springer-Verlag, New York, 1991).